COMPONENT PART NOTICE

THIS PAPER IS A COMPONENT PART OF THE FOLLOWING COMPILATION REPORT:

(TITLE): Proceedings of the International Conference on the Performance of Off-Road Vehicles and Machines (8th) Volume 1 Held at Cambridge, England on August 5-11, 1984

(SOURCE): International Society for Terrain-Veihcle Systems

TO ORDER THE COMPLETE COMPILATION REPORT USE AD-148 643.

THE COMPONENT PART IS PROVIDED HERE TO ALLOW USERS ACCESS TO INDIVIDUALLY AUTHORED SECTIONS OF PROCEEDINGS, ANNALS, SYMPOSIA, ETC. HOWEVER, THE COMPONENT SHOULD BE CONSIDERED WITHIN THE CONTEXT OF THE OVERALL COMPILATION REPORT AND NOT AS A STAND-ALONE TECHNICAL REPORT.

THE FOLLOWING COMPONENT PART NUMBERS COMPRISE THE COMPILATION REPORT:

COMPONENT PART NOTICE (CON'T)

AD#:	TITLE:
AD-P004 269	Leistungssteigerung und Verbesserung des Fahrkomforts Bei Selbstfahrenden Baumaschienen Durch Reduzierung Einsatbedingter Nick- und Hubschwingungen (Increase in Performance and Improvement of Ride Comfort of Self-Propelled Construction Machinery by Reducing Pitch and Vertical Vibration)
AD-P004 270	Stresses in Situ Generating by Bulldozers
AD-P004 271	Finite Element Analysis of Ground Deformation Beneath Moving Track Loads
AD-P004 271	A Rig for Testing the Soft Soil Performance of Track Systems
AD-P004 273	Die Abhaengigkeit der Bodentragfaehigkeit und der Zugkraft von der Abstandgroesse der Bodenplatten (The Dependence of Soil Bearing Capacity and Drawbar Pull on the Spacing between Track Plates)
AD-P004 274	The Dynamic Interaction between Track and Soil
AD-P004 275	Analysis of Ground Pressure Distribution Beneath Tracked Model with Respect to External Loading
AD-P004 276	A Comparison between a Conventional Method and an Improved Method for Predicting Tracked Vehicle Performance
AD-P004 277	Effect of Hitch Positions on the Performance of Track/Grouser Systems
AD-P004 278	Grouser Effect Studies
AD-P004 279	Ride Comfort of Off-Road Vehicles
AD-P004 280	Further Development in Ride Quality Assessment
AD-P004 281	Comparison of Measured and Simulated Ride Comfort for an Agricultural Tractor and Influence of Travel Speed and Tyre-Inflation Pressure on Dynamic Response
ADpP004 282	Characteristics of Fram Field Profiles as Sources of Tractor Vibration

Distribution/
Availability Codes
Dist | Avail and/or Special
A-1

PREDICTION OF IN-SAND TIRE AND WHEELED VEHICLE DRAWPAR PERFORMANCE

Gerald W. Turnage (Member, ISTVS)

U.S. Army Engineer Waterways Experiment Station, Vicksburg, Mississippi

ABSTRACT

In an appendix of the ISTVS 6th International Conference Paper, "A Synopsis of Tire Design and Operational Considerations Aimed at Increasing In-Soil Tire Drawbar Performance," the author developed a procedure for defining G_e, effective sand penetration resistance gradient. G_e was devised to approximate the value of G that predominated during a given tire pass, normalized to one type of frictional soil (selected as Yuma sand). G_e subsequently served as the soil strength term in sand-tire numeric N_{se}, which aimed at providing a normalized description of tire drawbar performance in different types of sands. Because the range of sand types included in the development of G_e and N_{se} was necessarily quite limited, the author suggested in the "Synopsis" paper that other investigators test the universality of relations involving N_{se} and tire drawbar performance by using tire test results obtained in a variety of sands.

In their ISTVS 7th International Conference paper, "An Assessment of the Value of the Cone Penetrometer in Mobility Prediction," A. R. Reece and J. O. Peca applied the N_{se} methodology for a quite different sand and obtained N_{se} versus tire drawbar performance results that were not described well by those in the "Synopsis" paper. This prompted a reexamination by the author of information in the "Synopsis" paper, an analysis of data presented in Reece and Peca's "Assessment" paper, and a reanalysis of a sizeable body of U. S. Army Engineer Waterways Experiment Station (WES) field data on wheeled vehicle performance tests in a variety of sands (all supplemented by new laboratory sand test data). The primary result of this work is definition of a new N_{sey} methodology that accurately predicts tire and wheeled vehicle drawbar performance in a very broad range of sand types and conditions, including those of the "Assessment" paper.

INTRODUCTION

To obtain best wheeled vehicle performance in sandy soils requires implementation of a rational methodology for selecting the most appropriate tires and then using those tires to best advantage. In turn, such a methodology requires an ability to predict accurately in-sand tire and wheeled vehicle performance. Using laboratory and field test results, this paper describes a useful methodology for predicting the drawbar performance of tires and wheeled vehicles operating in a broad range of sand types and conditions.

BACKGROUND

Drawbar pull and drawbar efficiency were selected to describe in-sand tire performance herein because (a) the amount of pull a powered wheel can develop is often of major concern in vehicle in-sand operations, and (b) the efficiency with which a given amount of pull is developed determines the input energy required, a major concern in today's energy-conscious world.

It has proved useful to describe in-sand tire performance by relating dimensionless tire performance terms to a dimensionless sand-tire prediction term, or numeric. Tire drawbar performance is described herein by the following two terms:

$$\text{Drawbar coefficient } (\mu) = DP/W \tag{1}$$

where

DP = drawbar pull, the "force available for external work in a direction parallel to the horizontal surface over which the (tire) is moving"[1]*

W = weight (load) on the tire

and

$$\text{Drawbar efficiency } (\eta) = \frac{DP\ v}{T\ \omega} \tag{2}$$

where

DP = drawbar pull

v = forward velocity of the wheel axle

T = torque input to the wheel

ω = rotation velocity of the torque input shaft

---

* Each raised number in the main text refers to a reference of the same number at the end of the text.

The sand-tire numeric N_s is defined as:

$$N_s = \frac{G(bd)^{3/2}}{W} \cdot \frac{\delta}{h} \tag{3}$$

where

G = sand penetration resistance gradient (described in the next paragraph)

b = unloaded tire section width

d = unloaded tire outside diameter

h = unloaded tire section height

δ = tire deflection (the difference between unloaded tire section height h and loaded tire section height, with each height measured as the tire rests on a flat, level, unyielding surface)

G is the average slope of the curve of soil penetration resistance C versus cone penetration depth, with C and cone depth measured within a specified soil layer (ordinarily the 0- to 15-cm layer). C is the force per unit cone base area required to penetrate a soil normal to its surface at 3.0 cm/sec with a right circular 30-deg-apex-angle cone of 3.23-sq-cm base area. (The equivalent of C in English units is cone index, CI.) Figure 1 shows sample recordings of C versus cone penetration depth for a laboratory-prepared sand test bed. Note that zero cone penetration depth is defined as occurring when the base of the 3.23-sq-cm cone is flush with the initial sand surface.

For simplification, drawbar performance is analyzed herein only at 20 percent slip--i.e., only μ_{20} and η_{20} data are considered. Use of this nominal slip value is meaningful because, as illustrated in Figure 2 (taken from Reference 2), 20 percent slip provides a reasonable balance of good in-sand tire μ and η performance (with somewhat greater weight given to μ) for a broad range of values of N_s .

EVOLUTION OF DRAWBAR PERFORMANCE PREDICTIONS BY N_s AND N_{sey}

Early Development of N_s

N_s was first defined by Freitag almost 20 years ago[3] by means of dimensional analysis of the results of laboratory dynamometer tests of single tires in air-dry Yuma sand (a desert sand taken from active dunes near Yuma, Arizona). Using data from Reference 4 for 10 tires tested in this sand, Figure 3 illustrates that N_s effectively consolidates μ_{20} test data to one well-defined relation (Figure 3a) and η_{20} data to another (Figure 3b) for very broad ranges of values of G , b , d , W , and δ/h . Thus, Figure 3 strongly supports the conclusion that N_s describes in-sand tire μ_{20} and η_{20} performance quite well--at least for air-dry Yuma sand.

In Reference 4, the relation of drawbar pull data to N_s was also examined for tests "conducted on coarse-grained soils in various parts of the world with a variety of military vehicles." In these field tests, sand "usually was moist or even wet; drawbar-pull tests usually were not run at a controlled slip but were made at several levels of pull with only the data relevant to the maximum pull recorded for each test; and no

special provisions were made to control differential wheel slip, dynamic weight transfer, or steering forces." Figure 4 illustrates, as would be expected, (a) that the μ_{20} versus N_s relation defined by these field test data shows much smaller values of μ_{20} at corresponding values of N_s than does the single-tire laboratory relation of Figure 3a, and (b) that the field relation exhibits substantially more data scatter than does the laboratory relation.* (Data from tests at sand moisture contents only up to about 7 percent are shown in Figure 4.) The field relation in Figure 4 was considered sufficiently well defined, however, to "offer the basis for a tentative performance prediction system . . . for vehicles operating in dry-to-moist sands."

For a number of years this "tentative performance prediction system" was accepted as workable, although it was recognized that the system had potential for further refinement. Such refinements were made piecemeal and in an evolutionary manner, primarily because of the lack of data for defining in detail a range of physical properties of the sands for which tire and wheeled vehicle drawbar performance data were available. Events of the past few years have caused a renewed interest, however, in refining and improving the drawbar performance versus sand-tire numeric methodology for wheeled vehicles. The remainder of this paper describes development of such a methodology, first taking into account some insights gained in earlier studies of the influence of sand type on single-tire drawbar performance.

First Considerations of Two Sand Types

In addition to single-tire tests in air-dry Yuma sand, WES also conducted a smaller, but significant, number of laboratory tests in air-dry mortar sand (a coarser-grained riverbed sand). Figure 5a uses data from tests of five tires in mortar sand, together with the μ_{20} versus N_s curve from Figure 3a for Yuma sand, to demonstrate that these tires developed consistently smaller values of μ_{20} in mortar than in Yuma sand at corresponding values of N_s.

In 1972, Reference 5 attempted to account for this difference by using the relations of G to relative density (D_r) for the two sands, defined from Reference 6. For air-dry mortar sand:

$$D_r = 75.0 \log G + 39.3 \tag{4}$$

and for air-dry Yuma sand:

$$D_r = 71.1 \log G + 51.6 \tag{5}$$

where

$$D_r = \frac{e_{max} - e}{e_{max} - e_{min}} \times 100\text{, percent} \tag{6}$$

---

* For simplicity, all drawbar coefficient data considered herein are designated μ_{20} data, although μ in the wheeled vehicle field tests was sampled at the near-maximum-pull level, not necessarily 20 percent slip. Also, for brevity, tire drawbar performance in several subsequent figures is defined only in terms of μ_{20}. Performance is described in terms of both μ_{20} and η_{20} in appropriate concluding figures.

e_{max} and e_{min} are void ratios for the loosest and densest sand states, respectively, and e is void ratio for the before-tire-pass sand condition. A given value of mortar sand G (G_M in Figure 5) was converted to Yuma sand G (G_Y) by first determining the mortar sand D_r value in Equation 4 and then using that same D_r value to solve for Yuma sand G in Equation 5. This use of D_r as the intermediate soil parameter in translating G values between different sands appeared to produce the desired result, as evidenced in Figure 5b by the shift of the mortar sand tire test data to locations clustered about the μ_{20} versus N_s curve for Yuma sand. Reference 5 recognized, however, that use of D_r as described above must be considered tentative, and recommended "that tests be conducted in several additional sands so that the relative density approach . . . can be further verified."

In 1975, Reference 7 reported drawbar performance results from a later series of tests in air-dry mortar sand, these conducted with four 9.00R20 radial ply tires (each different in terms of tread design and other construction features), plus two 9.00-20 bias-ply tires (one with nondirectional cross-country tread, the other with tread buffed smooth). Tests for each tire were conducted over a range of wheel loads and tire deflections, and at two levels of G, approximately 2.2 and 5.5 MPa/m. For tire deflections of 15 and 35 percent, Figure 6a shows that the relation of μ_{20} to N_s separated as a function of G. Further, Figure 6b shows that the relation of μ_{20} to $(N_s)_Y$ for these test data also separated by G_Y (where G_Y values in $(N_s)_Y$ were obtained by Equations 4 and 5 and the process described in the previous paragraph). In attempting to account for this separation, Reference 7 noted that "Ideally, the G value to use in describing tire performance for a given (tire) pass is the value that predominated during that pass. For first pass, this value lies between the 0- and 1-pass values"--i.e., between the before- and after-first-pass values. Examination of mortar sand tire test data showed "that G changes with tire traffic in a funnel-shaped pattern" like that shown in Figure 6c, and "indicated that the best G value for describing first-pass, 20-percent-slip tire performance is G at "pass number" 0.75 (hereafter termed $G_{0.75}$). That is, G should be weighted 3:1 toward its after-first-pass value." Figure 6d shows the well-defined relation obtained for μ_{20} versus N_s', where $N_s' = \frac{G_{0.75}(bd)^{3/2}}{W} \cdot \frac{\delta}{h}$.
While the μ_{20} versus N_s' relation collapsed the mortar sand test data for the six 9.00x20 tires quite well, the central curve in Figure 6d is notably different from the one in Figure 3a for Yuma sand. The thrust of the analysis in Reference 7 was not directed at accounting for the influence of sand type on tire drawbar performance. However, Reference 7 recognized that "Clearly, more work is needed to develop techniques for describing sand soil strength that changes significantly with tire traffic."

A First-Cut, More General N_s Methodology

In 1978, Reference 8 attempted to define a methodology to satisfy the two needs demonstrated in Figures 5 and 6--i.e., to define a means (a) for translating G values between different sand types, and (b) for describing the effective (predominant) during-tire-pass value of G. This methodology was applied by means of the nomogram shown in Figure 7.

The aim of the nomogram was to define G_e, "effective sand penetration gradient, the value of G that predominated during a given tire pass, normalized to one type of frictional soil (selected as Yuma sand)."

Use of the nomogram required known before-tire-pass values of G and of D_r (G_b and D_{rb}, respectively), and involved the following steps (identified by circled numbers in Figure 7):

Step 1: For the sand of interest (taken as mortar sand in Figure 7a), determine for G_b the corresponding value of D_{rb}.

Steps 2 and 3: For the tire b/d value of concern (0.29 in Figure 7b, for example), translate the D_{rb} value of step 1 from Figure 7a to 7b (shown as a dot in the example). In Figure 7b, use the family of curves that relate D_{rb} to D_{re} (effective relative density) as a function of tire b/d to estimate D_{re}.

Steps 4 and 5: Translate D_{re} of step 3 for the sand of interest to D_{re} for Yuma sand (step 4), and then to G_e for Yuma sand (step 5).

G_e from step 5 was then used as the soil strength term in

$N_{se} = \frac{G_e(bd)^{3/2}}{W} \cdot \frac{\delta}{h}$, and N_{se} was related to tire drawbar performance terms $\mu_{20} \tan \phi_{70}$ and $\eta_{20} \tan \phi_{70}$. The rationale for using $\tan \phi_{70}$ (tangent of sand internal friction angle from a direct shear test at 70 percent relative density) as a multiplier of μ_{20} and η_{20} was that (a) D_{rb} tends toward a D_{re} value of about 70 percent for common tire shapes (b/d values from about 0.2 to 0.3), particularly with repeated transformations of D_{rb} to D_{re} to correspond to multiple tire passes, and (b) the products $\mu_{20} \tan \phi_{70}$ and $\eta_{20} \tan \phi_{70}$ appeared, in conjunction with N_{se}, to provide a normalized description of tire drawbar performance for the three frictional soils considered in Reference 8 (Yuma and mortar sands, plus a finely crushed basalt used as lunar soil simulant, LSS, described in Reference 9).

Figure 8 shows the relations (a) of μ_{20} to N_s and (b) of $\mu_{20} \tan \phi_{70}$ to N_{se} based on test results in Yuma sand for the same 10 tires as in Figure 3a, in mortar sand for the same 11 tires as in Figures 5 and 6, and in LSS for one tire-like wheel. (This wire-mesh wheel was evaluated for use on the lunar rover vehicle by testing the wheel in the rather exotic LSS. The two asterisks of Figure 7a define coordinates of D_r and G for the two LSS test conditions.) For the test data considered, the relation of $\mu_{20} \tan \phi_{70}$ to N_{se} in Figure 8b is considerably better defined than is that of μ_{20} to N_s in Figure 8a. While the Figure 8b relation appeared promising, Reference 8 "recognized that the range of frictional soil types considered . . . is limited; thus it is hoped that other investigators will test the universality of the $\mu_{20} \tan \phi_{70}$ and $\eta_{20} \tan \phi_{70}$ versus N_{se} relations using tire test results obtained in a variety of frictional soils."

In 1981, References 10 and 11 applied the methodology described in Figures 7 and 8 to drawbar performance data obtained with a 6.00-16, 2-PR treadless (smooth) tire in air-dry Cresswell sand. For this tire-sand combination, Figure 9 shows that the $\mu_{20} \tan \phi_{70}$ versus N_{se} relation obtained was very different from that obtained in Figure 8b. Clearly, the $\mu_{20} \tan \phi_{70}$ and $\eta_{20} \tan \phi_{70}$ versus N_{se} methodology was shown not to successfully treat all sand tire situations, and the need was established for analyzing a broad range of sand types and conditions in one study. A description of that analysis follows.

A New N_{sey} Methodology for a Broad Range of Sand Types and Conditions

The Test Sands. Two major limitations in the WES analyses described to this point are that (a) only two ordinary test sands were considered (Yuma and mortar sand--the exotic LSS is hereafter not considered), and (b) these sands were each used only air-dry in single-tire testing. The new analysis considers 10 sands--the Yuma, mortar, and Cresswell sands, plus seven other sands for which vehicle field drawbar test data were available (six sands from References 4 and 12, one from Reference 13). A separate value of sand moisture content was reported in References 12 and 13 for each wheeled vehicle test; tests at moistures from 1 to 7 percent are considered herein.

A necessary first step in the analysis was to obtain samples of approximately 100 kg each for the 10 test sands. In this regard, particular thanks are extended to Dr. A. R. Reece for supplying the needed sample of Cresswell sand (the sand used in References 10 and 11), and to Dr. L. I. A. C. Grosjean, Etablissement Technique d'Angers, for supplying sand samples from beaches at La Turballe and at Suscinio, France (two of the test sites in References 4 and 12). Samples of the Yuma and mortar sands were obtained from large stockpiles at WES, and samples of the remaining five sands were obtained in re-visits to wheeled vehicle test sites in the United States.

A major concern in the new analysis was how closely the 10 sand samples matched the sands actually used in the tests of single tires or wheeled vehicles reported in References 4, 10, 11, 12, and 13. One means of evaluating this was to compare the original grain-size distribution curves shown in these references with the corresponding curves shown in Figure 10 for the sand samples that were used in 1983 WES soils laboratory testing. Results of this comparison are shown in Table 1 for grain-size diameters at the 10, 30, 50, 70, and 90 percent finer by weight levels. As expected, the original and the 1983 curves matched very closely for the Yuma and mortar sands (WES laboratory test sands). For Paw Paw Island sand, the original and 1983 curves are one and the same. For Cresswell sand, there is a noticeable difference between the original and 1983 curves.

The remaining six sands were tested in the field during 1958-1961, as reported in Reference 12 (1963). It was anticipated that the passage of some 20-25 years time, plus inability to locate precisely some of the original test sites, could cause substantial differences between the original and 1983 distribution curves, at least for some of the six Reference 12 sands. As it turned out, the original and the 1983 curves showed almost perfect agreement for the Padre Island site, very close agreement for the Mississippi River Bridge site, somewhat less agreement for the La Turballe and the two National Seashore Headquarters sites, and least agreement (by a considerable margin) for the Suscinio site. Implications of comparisons between the original and the 1983 sand grain diameters as described in Table 1 are discussed later in the analysis.

Relations Among G, D_r, and Sand Moisture Content. In analyzing data for the 10 sand samples, it was recognized, first, that D_r appeared not to be suitable for use as an intermediate soil parameter in translating between sand types. (Recall from Figures 6a and 6b that separation of μ_{20} data for the Yuma and mortar sands was not alleviated

by the use of D_r in a translation role.) However, D_r did appear promising for use in a standardized description of the change in sand strength that occurs during a given tire pass. (Note that Figure 7b uses D_r in this role to describe the same process somewhat more crudely described in Figure 6c.) Further, D_r has the advantageous characteristics (a) of increasing in value as G increases, decreasing as G decreases, and (b) of taking values within the same range (0 to 100 percent) for all sands.

To develop the desired standardized description, the relation between G and D_r was determined for each of the 10 sand samples at sand moisture conditions at least from air-dry to 7 percent moisture. Additionally, measurements of G and D_r were obtained for the Yuma and Cresswell sands at a fully saturated condition and for Cresswell sand at 0.1 percent moisture content.

Figure 11 shows relations among G, D_r, and sand moisture content representative of those obtained for the 10 sand samples. For Yuma sand, this figure illustrates that the G versus D_r relation is described by

$$D_r = a_1 \log G + a_2 \tag{7}$$

where a_1 is a constant for a given sand, and a_2 changes value as a function of sand moisture content. Note in Figure 11 that a_2 decreases as sand moisture content increases from air-dry to about 7 percent (this same pattern was obtained for all the test sands), but a_2 increases markedly as moisture increases from about 7 percent to the fully saturated condition (this pattern was also obtained for Cresswell sand).

Figure 12 illustrates the relations (a) of a_2 to sand moisture content, and (b) of G (at $D_r = 70$ percent) to sand moisture content that were obtained for the Yuma and Cresswell sands. For each of the 10 sand samples, the pattern of change in a_2 with change in moisture from air-dry to 7 percent was similar to that shown by the dashed curves in Figure 12--i.e., for each sand, a_2 decreased semilogarithmically as moisture increased from air-dry to about 2 percent, and then continued to decrease, but at a fast-diminishing rate until a minimum a_2 value was obtained at about 7 percent moisture. For the Yuma and Cresswell sands, a_2 increased rapidly as sand moisture increased beyond about 7 percent.

The influence on G caused by this pattern of change in a_2 with sand moisture content is seen by rearranging Equation 7 to

$$G = \text{antilog} \frac{D_r - a_2}{a_1} \tag{8}$$

Thus, for each of the 10 sand samples (constant a_1) and any constant level of D_r, G attained a maximum value at minimum a_2--i.e., at about 7 percent moisture content. Further, based on data for two of the test sands (Yuma and Cresswell), it appears that, for a given sand and constant D_r, G decreases rapidly as sand moisture content increases beyond about 7 percent.

Table 2 summarizes in columns 1-9 for each of the 10 sand samples the relation of D_r to G obtained in 1983 WES laboratory testing at sand moisture contents from air-dry to 7 percent. (Values in other columns of Table 2 will be discussed subsequently.) Note in column 2 that each listed value of air-dry sand moisture content was obtained

in the WES soils laboratory after a given sand sample remained undisturbed for at least seven days. These at-WES air-dry moisture contents do <u>not</u> necessarily correspond to air-dry moisture contents at other sites.

<u>Prediction of During-Tire-Pass G_e</u>. To predict G_e for the 10 test sands required implementation of both (a) the relations among G, D_r, and sand moisture content (summarized in columns 1-9 of Table 2), and (b) the relations among G_b, tire shape factor b/d, and G_e shown in Figure 13. A three-step process is involved:

(1) Use Equation 8 to estimate D_{rb} (from known values of G_b, a_1, and a_2).

(2) Obtain D_{re} from Figure 13 (using D_{rb} from step 1 and known b/d).

(3) Compute $G_e = \text{antilog} \dfrac{D_{re} - a_2}{a_1}$ (using the same values of a_1 and a_2 as in step 1).

Before applying the above process, it is useful to examine the relation in Figure 13. The shape of each curve in Figure 13a is the same as in Figure 7b for b/d values of about 0.2 and larger. For smaller b/d values, the curves in Figure 13a reflect recent analysis of single-tire drawbar test data in Yuma sand using the 1.75-26 bicycle and 4.00-20, 2-PR tires (b/d values of 0.068 and 0.150, respectively) not considered in Reference 8.*

In agreement with Reference 7 and with Figure 6c herein, D_{re} in Figure 13a reflects the condition obtained at tire pass number 0.75--i.e., first-pass D_{re} is considered weighted 3:1 toward the after-first-pass condition. For two powered-wheel tire passes, the appropriate D_{re} value is for tire pass 1.75; for three tire passes, 2.75; and for four tire passes, 3.75. The relation in Figure 13a was successively applied to obtain D_{re} values for tire pass multiples of 0.75; D_{re} values for tire passes 2, 3, and 4 were then obtained by interpolation as needed.

Detailed application of the D_{rb}, b/d, D_{re} relation for a given all-axles-powered wheeled vehicle would require that a separate value of G_e be determined for each axle, and that these G_e values then be averaged to determine G_e for the overall vehicle. Figures 13b, 13c, and 13d avoid this cumbersome process by reflecting averaged values of D_{re} for tire passes 1 and 2, passes 1 through 3, and passes 1 through 4, respectively. For a given 4x4, 6x6, or 8x8 vehicle, then, use of the

---

* In Reference 8, μ_{20} (and η_{20}) values for all the tires considered reflected a mechanical/electrical correction to negate dynamometer carriage acceleration forces developed in the single-tire, programmed-increasing-slip tests. No such correction had been in use during tests of the 1.75-26 bicycle and 4.00-20, 2-PR tires reported in Reference 4. However, for a number of single tires tested over a broad range of N_s values, acceleration-corrected μ_{20} from Reference 4 has been determined to be smaller than uncorrected μ_{20} by a near-constant 0.045. For both the 1.75-26 and the 4.00-20 tires, the acceleration-corrected μ_{20} values used herein were obtained by subtracting 0.045 from μ_{20} values previously uncorrected for carriage acceleration.

single appropriate relation in Figure 13b, 13c, or 13d produces a single D_{re} value and a subsequent value of G_e very close to that obtained by treating each axle singly.

Use of G_e in N_{se}. The intended application of G_e, as defined by the three-step process described earlier, was to serve as the soil strength term in sand-tire numeric $N_{se} = \frac{G_e (bd)^{3/2}}{W} \cdot \frac{\delta}{h}$, such that N_{se} would collapse both single-tire and wheeled-vehicle drawbar data for a broad range of sand conditions to a single relation for a given sand type. The success of G_e in this role is illustrated, first, in Figures 14a and 14b which show for 10 single tires and for three 4x4 vehicles, all tested in air-dry Yuma sand, that all the test data cluster closely about the same central μ_{20} versus N_{se} relation.

N_{se} was also determined to be more effective than N_s in consolidating μ_{20} data for each of the nine other test sands, in each case producing (as expected) a separate μ_{20} versus N_{se} relation. Figure 15 shows representative results, using data (a) from tests of a single 6.00-16, 2-PR tire in air-dry Cresswell sand and (b) from tests of four wheeled vehicles in moist sand at the Padre Island site.

Normalization of G_e to G_{ey}. Having developed a means to predict G_e, it remained to develop a means for normalizing G_e to one sand type, selected as Yuma sand. Analyses were made involving a number of parameters descriptive of physical properties of the 10 sand samples, with best results obtained by application of the relations shown in Figure 16.

In Figure 16, three sand parameters are involved--penetration resistance gradient (G), sand compactibility (D'), and sand grain median diameter (d_{50}). Compactibility is defined as

$$D' = \frac{e_{max} - e_{min}}{e_{min}} \times 100, \text{ percent} \tag{9}$$

and d_{50} (sand grain diameter for which 50 percent of the sand sample is finer by weight) is read directly from a sand's grain-size distribution curve. In Figure 16, subscript x denotes sand x, and subscript y denotes Yuma sand. For a given sand x, known values of D'_x/D'_y and $(d_{50})_x/(d_{50})_y$ are used in Figure 16 to determine corresponding values of $(G_{ex}/G_{ey})_{D'}$ and $(G_{ex}/G_{ey})_{d_{50}}$, respectively. A given value of G_e for sand x (G_{ex}) is then normalized to the corresponding value for Yuma sand (G_{ey}) by the relation

$$G_{ey} = G_{ex} \div (G_{ex}/G_{ey}) \tag{10}$$

where

$$G_{ex}/G_{ey} = (G_{ex}/G_{ey})_{D'} \times (G_{ex}/G_{ey})_{d_{50}} \tag{11}$$

For use in normalizing G_{ex} to G_{ey}, the curves in Figure 16 exhibit expected trends. A given sand of high compactibility requires less force for its displacement than does one of low compactibility at the same relative density. Thus, for $D'_x/D'_y > 1$ (all other conditions constant), G_{ex} must be increased for normalization to G_{ey}. This is accomplished by taking the appropriate value of $(G_{ex}/G_{ey})_{D'} < 1$ from Figure 16, applying this value in Equation 11, and then using Equation 10. (For $D'_x/D'_y < 1$, $(G_{ex}/G_{ey})_{D'} > 1$ and G_{ex} is decreased in normalization to G_{ey}.)

Note, also, that the penetration resistance of a sand with large-diameter grains is greater than that of one with smaller grains (all other conditions constant). Thus, for $(d_{50})_x/(d_{50})_y > 1$, $(G_{ex}/G_{ey})_{d_{50}} > 1$ and G_{ex} is decreased in normalization to G_{ey}. (For $(d_{50})_x/(d_{50})_y < 1$, G_{ex} is increased in normalization to G_{ey}.)

Use of G_{ey} in N_{sey}. Having determined the value of G_{ey} for a particular sand x, the next step is to use G_{ey} in $N_{sey} = \frac{G_{ey}(bd)^{3/2}}{W} \cdot \frac{\delta}{h}$ to predict in-sand μ_{20} and η_{20} tire and wheeled vehicle performance. The success of G_{ey} in this role is illustrated in the following comparisons.

In Figure 17a, data for all of the single-tire tests considered herein for the Yuma, mortar, and Cresswell sands cluster about the same μ_{20} versus N_{sey} curve obtained earlier for Yuma sand in Figures 14a and 14b. (Note that $N_{sey} = N_{se}$ for Yuma sand only.) In Figure 17b, single-tire test data for these three sands all cluster about the same η_{20} versus N_{sey} relation. Note further that, based on results from the same laboratory single-tire tests, data collapse about the two relations involving N_{sey} in Figure 17 is considerably better than that about corresponding relations in Figure 18 involving N_s.

In Figure 19, the wheeled-vehicle test data for six sandy field test sites show much less data scatter about the central μ_{20} versus N_{sey} curve (the same curve as in Figures 14 and 17a) than do corresponding data for the same test sites in Figure 4 about the central curve of μ_{20} versus N_s.*

Based on Figures 17 and 19, N_{sey} is demonstrated to be very effective in consolidating single-tire and wheeled-vehicle μ_{20} data to one relation, η_{20} data to another. Remarks modifying this general conclusion need to be made, however, relative primarily to one of the laboratory test sands in Figure 17 (Cresswell sand) and to the one field test sand not shown in Figure 19 (Suscinio sand).

Some Strengths and Limitations of the N_{sey} Methodology. First, regarding the Cresswell sand, determination of its G_{ey} values in Figure 17 was made using as input data one set of G values gleaned from References 10 and 11, plus values of a_1, a_2, D', and d_{50} from the 1983 WES laboratory tests of the Cresswell sand sample (using

* No η_{20} versus N_{sey} relation is shown in Figure 19 because measurements of η_{20} were not obtained in any of the wheeled vehicle tests considered herein.

a_2 at the WES air-dry condition). There was interest in determining how these predicted values of G_{ey} (and of N_{sey}) compared with those obtained by using the same set of G values, together with input values of a_1, a_2, D', and d_{50}, obtained from References 10, 11, and 14. Table 3 summarizes this comparison.

For the 11 air-dry Cresswell sand test conditions considered, the major conclusion from Table 3 is that, although two quite different sets of input values of a_1, a_2, D', and d_{50} were used (see the two footnotes of Table 3), nearly identical values of G_{ey} and of N_{sey} were predicted (compare results in columns 9 and 10 with those in columns 14 and 15). This close agreement reflects that the overall process for translating values of G to G_{ey} (summarized in the first footnote of Table 3) is reasonably robust. That is, based on the comparison in Table 3, the G-to-G_{ey} prediction process appears not to be unduly influenced by even fairly sizeable variations in values of its required input parameters.

This tentative conclusion is supported by the wheeled vehicle field relations shown in Figures 4 and 19. For the first five sands in the legends of these two figures, the sand samples used in defining values of a_1, a_2, D', and d_{50} by 1983 WES laboratory testing were like the sands used in actual 1958 to 1961 field testing only to varying degrees—see Table 1. (For the sixth sand, from the Paw Paw Island site, the 1983 sand sample was taken from the precise location of field testing.) For the first five sands, taking this discontinuity between sample and test sands into account, the improvement in the relation of μ_{20} versus N_{sey} in Figure 19 versus the μ_{20} versus N_s relation in Figure 4 is rather remarkable, even with one significant caveat: the μ_{20} versus N_{sey} relation obtained for Suscinio sand (not shown in Figure 19) is considerably different from that shown in Figure 19 for the six other field test sands (it is displaced far to the left).

There are two principal possibilities for explaining what at first seems to be the atypical μ_{20} versus N_{sey} behavior of the Suscinio data. First, it is possible that one or more sand parameters needed in the process for translating G to G_{ey} have been omitted. The process described herein is the one that was determined to make the G-to-G_{ey} translation best for the test data examined, based on analysis not only of the sand parameters now included in the process, but also of several other parameters initially considered potentially important (coefficient of uniformity $C_u = d_{60}/d_{10}$, angle of internal friction, etc.). Still, modifications might substantially improve the G-to-G_{ey} translation process, and such modifications are welcomed.

The second, and much more likely, reason for the μ_{20} versus N_{sey} behavior of the Suscinio sand relates to the fact that, of the 10 sand samples used in 1983 WES laboratory testing, Suscinio's grain diameter distribution showed least agreement with its corresponding original distribution, by a large margin—see Table 1. Thus, it was not surprising, when the $D_r = 141.0 \log G + a_2$ laboratory relation for Suscinio sand was applied to Suscinio field values of G, that values of D_r considerably larger than 100 percent were obtained in some cases. (This did not occur with the nine other sands.) Note, also, from Table 1 that the Suscinio field sand was considerably less coarse than the 1983 Suscinio sample sand (which included almost as much gravel as sand—see Figure 10). In fact, from Table 1, the Suscinio field sand's overall distribution of d values is approximated just as well by the 1983 La Turballe laboratory sample (from the low side) as it is by the Suscinio laboratory sample (from the high side). (Prediction of Suscinio G_{ey} values by using for input

Suscinio field G values and La Turballe laboratory a_1 , a_2 , D', and d_{50} values produced a Suscinio μ_{20} versus N_{sey} relation very closely approximated by the relation in Figure 17.) Finally, note that the good fit of the Suscinio data in the μ_{20} versus N_s relation of Figure 4 further indicates that characteristics of the Suscinio sand, as encountered on-site and measured at least by G , were not foreign to those of the six other sands in Figure 4.

The above observations suggest that, for the Suscinio beach site, the discontinuity between 1983 sample sand and 1959 field sand was simply too large to overcome in using a_1 , a_2 , D' , and d_{50} values from the sample sand to describe drawbar performance in the field sand. These observations also lead to the caveat that it remains to be determined how coarse a sand must be for the N_{sey} relations not to apply. (Sands at least as coarse as the La Turballe sand are successfully treated by N_{sey} .) A second caveat is that a substantial amount of laboratory testing is necessary to define the input values of a_1 , a_2 , D' , and d_{50} required by the process for translating G to G_{ey} for use in N_{sey} (particularly to define a_1 and a_2 for the range of values of D_r and sand moisture content of possible concern). If the user is not restricted by these two caveats, the N_{sey} relations of Figures 17 and 19 are useful now in predicting drawbar performance with better accuracy than do the N_s relations of Figures 18 and 4. If the above caveats negate use of the N_{sey} relations, the μ_{20} versus N_s relation of Figure 4 is still judged sufficiently well defined to offer the basis for a useful wheeled vehicle drawbar performance system.

SUMMARY AND CONCLUSIONS

To summarize, a five-step process was developed for predicting tire and wheeled vehicle μ_{20} and η_{20} performance for a given sand and sand moisture content, described as follows:

(1) Use Equation 7 to estimate D_{rb} (from known values of G_b , a_1 , and a_2).

(2) Obtain D_{re} from Figure 13.

(3) Compute $G_e = \text{antilog} \dfrac{D_{re} - a_2}{a_1}$. For sand x , this is G_{ex} .

(4) Convert G_{ex} to G_{ey} by use of Figure 16 and Equations 11 and 10.

(5) Use G_{ey} in N_{sey} and the relations in Figure 17 to predict μ_{20} and η_{20} .

Relations of μ_{20} and η_{20} to N_{sey} now offer better prediction accuracy than do those of μ_{20} and η_{20} to N_s for a broad range of sand types and strengths, and for sand moisture contents up to about 7 percent. Implementation of the N_{sey} relations is limited, however, by two caveats: (a) the exact range of sand types for which the N_{sey} relations are applicable remains to be determined (sands from at least as fine as the Yuma sand to at least as coarse as the La Turballe sand considered herein are successfully treated by N_{sey}), and (b) substantial laboratory testing is necessary to define values of a_1 , a_2 , D' , and d_{50} , which are required as input by the process for defining G_{ey} for use in N_{sey} . Further work is needed to minimize or eliminate the influence of these two caveats. For now, with proper account taken of their

limitations, either the N_{sey} or the N_s methodology can be employed to predict in-sand tire and wheeled vehicle drawbar performance with useful accuracy.

REFERENCES

1. Meyer, M. P. et al., "International Society for Terrain-Vehicle Systems Standards," Journal of Terramechanics, Vol 14, No. 3, 1977, pp 153-182.

2. Melzer, K.-J., "Power Requirements for Wheels Operating in Sand," Proceedings of the International Conference of CIGR on the Perspectives of the Development of Agricultural Tractor Design, Vol 1, p 197, Warsaw, Poland.

3. Freitag, D. R., "A Dimensional Analysis of the Performance of Pneumatic Tires on Soft Soils," Technical Report No. 3-688, August 1965, U. S. Army Engineer Waterways Experiment Station, CE, Vicksburg, Miss.

4. Turnage, G. W., "Performance of Soils Under Tire Loads; Application of Test Results to Tire Selection for Off-Road Vehicles," Technical Report No. 3-666, Report 8, September 1972, U. S. Army Engineer Waterways Experiment Station, CE, Vicksburg, Miss.

5. Patin, T. R., "Performance of Soils Under Tire Loads; Extension of Mobility Prediction Procedures to Rectangular Cross-Section Tires in Coarse-Grained Soil," Technical Report No. 3-666, Report 7, April 1972, U. S. Army Engineer Waterways Experiment Station, CE, Vicksburg, Miss.

6. Melzer, K.-J., "Measuring Soil Properties in Vehicle Mobility Research; Relative Density and Cone Penetration Resistance," Technical Report 3-652, Report 4, July 1971, U. S. Army Engineer Waterways Experiment Station, CE, Vicksburg, Miss.

7. Turnage, G. W., "In-Soil Tractive Performance of Selected Radial- and Bias-Ply Tires," Paper No. 76-1520, December 1976, American Society of Agricultural Engineers, St. Joseph, Mich.

8. Turnage, G. W., "A Synopsis of Tire Design and Operational Considerations Aimed at Increasing In-Soil Tire Drawbar Performance," Proceedings, 6th International Conference, International Society for Terrain-Vehicle Systems, Vol II, pp 757-810.

9. Melzer, K.-J., "Performance of the Boeing LRV Wheels in a Lunar Soil Simulant; Effects of Speed, Wheel Load, and Soil," Technical Report M-71-10, Report 2, December 1971, U. S. Army Engineer Waterways Experiment Station, CE, Vicksburg, Miss.

10. Peca, J. O. and Reece, A. R., "Tyre Performance on Submerged Sand," Proceedings, 7th International Conference, International Society for Terrain-Vehicle Systems, Vol II, pp 755-796.

11. Reece, A. R. and Peca, J. O., "An Assessment of the Value of the Cone Penetrometer in Mobility Prediction," Proceedings, 7th International Conference, International Society for Terrain-Vehicle Systems, Vol III, pp A1-A33.

12. Rush, E. S., "Trafficability of Soils; Tests on Coarse-Grained Soils with Self-Propelled and Towed Vehicles 1958-1961," Technical Memorandum No. 3-240, Seventeenth Supplement, May 1963, U. S. Army Engineer Waterways Experiment Station, CE, Vicksburg, Miss.

13. Schreiner, B. G., Moore, D. W., and Grimes, K., "Mobility Assessment of the Heavy Expanded Mobility Tactical Truck - Initial Production Vehicles," Technical Report (in preparation), U. S. Army Engineer Waterways Experiment Station.

14. Peca, J. O., "Traction on Sand," unpublished Ph.D. Thesis, August 1983, Department of Agricultural Engineering, University of Newcastle upon Tyne.

NOTATION

a_1, a_2	Constant and variable, respectively, in the equation $D_r = a_1 \log G + a_2$ for a given sand over a range of sand moisture contents
b	Unloaded tire section width
C	Soil penetration resistance
C_u	Coefficient of uniformity
CI	Cone index
d	Unloaded tire outside diameter
d_{50}, $(d_{50})_x$, $(d_{50})_y$	Median diameter of sand grains, d_{50} of sand x, d_{50} of Yuma sand
D', D'_x, D'_y	Compactibility, compactibility of sand x, compactibility of Yuma sand
D_r, D_{rb}, D_{re}	Relative density, before-tire-pass relative density, effective (predominant during-tire-pass) relative density
DP, DP_{20}	Drawbar pull, drawbar pull at 20 percent slip
e, e_{max}, e_{min}	Before-tire-pass sand void ratio, maximum sand void ratio, minimum sand void ratio
G, G_b, G_e, G_{ex}, G_{ey}	Sand penetration resistance gradient, before-tire-pass G, effective (predominant during-tire-pass) G, G_e for sand x, G_e for Yuma sand
h	Unloaded tire section height
i	Slip
N_s, N_{se}, N_{sey}	Sand-tire numerics $N_s = \frac{G(bd)^{3/2}}{W} \cdot \frac{\delta}{h}$, $N_{se} = \frac{G_e(bd)^{3/2}}{W} \cdot \frac{\delta}{h}$, and $N_{sey} = \frac{G_{ey}(bd)^{3/2}}{W} \cdot \frac{\delta}{h}$

T	Torque input to wheel
v	Forward velocity of wheel axle
W	Load on a single tire
δ	Tire deflection (under load)
μ, μ_{20}	Drawbar coefficient, drawbar coefficient at 20 percent slip
η, η_{20}	Drawbar efficiency, drawbar efficiency at 20 percent slip
ω	Rotation velocity of the torque input shaft

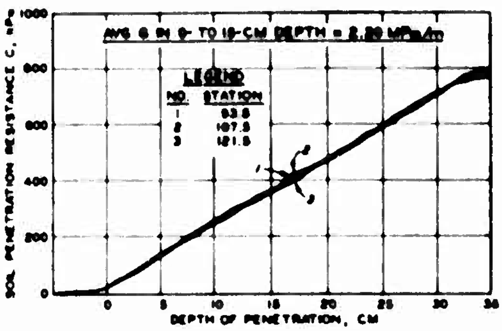

Figure 1. Sample recordings of cone penetration tests in a sand test bed

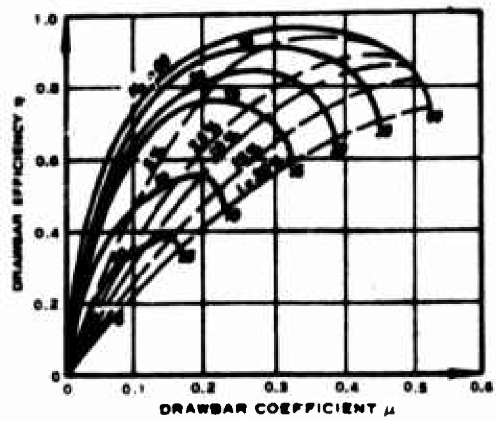

Figure 2. Relations of μ and η to N_s and slip (i) for pneumatic tires operating in a frictional sand (adapted from Reference 2)

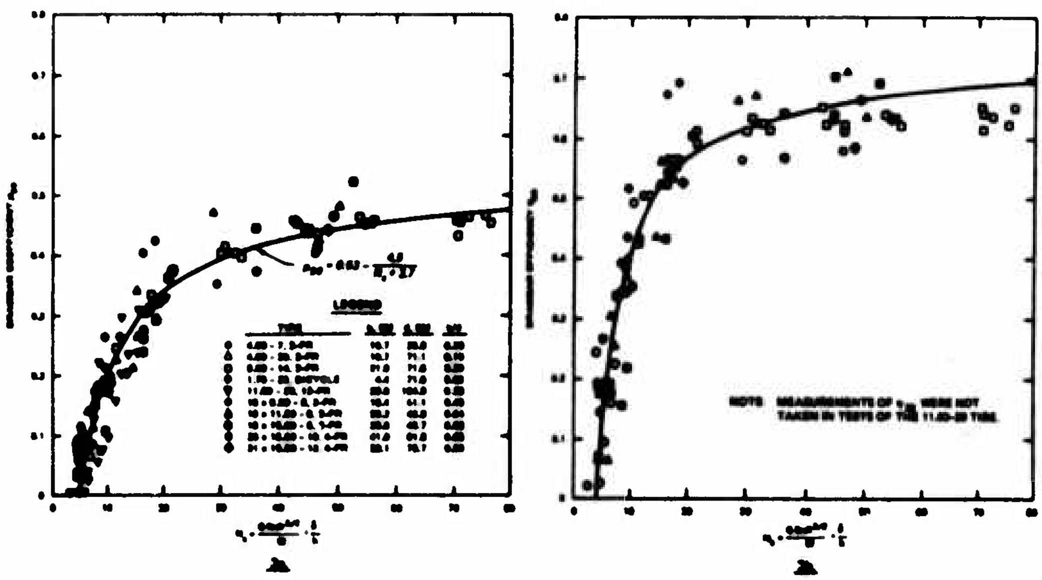

Figure 3. Relations of μ_{20} and η_{20} to N_s for ten single pneumatic tires tested in air-dry Yuma sand (values of G from 0.62 to 7.52 MPa/m, W from 0.41 to 20.02 kN, and δ/h from 0.15 to 0.35)

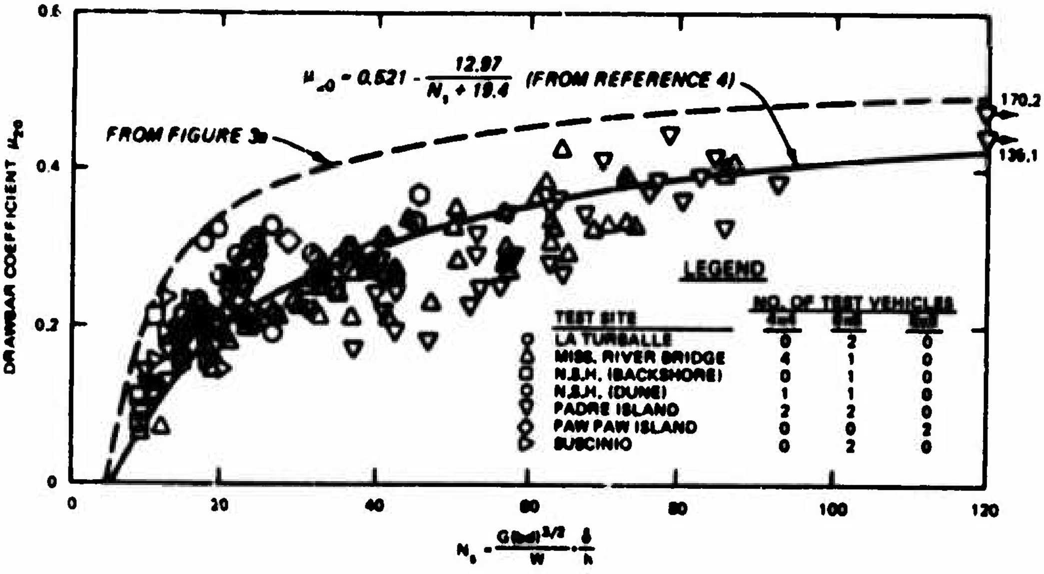

Figure 4. Relation of μ_{20} to N_s for tests with a variety of wheeled vehicles at seven sandy field sites

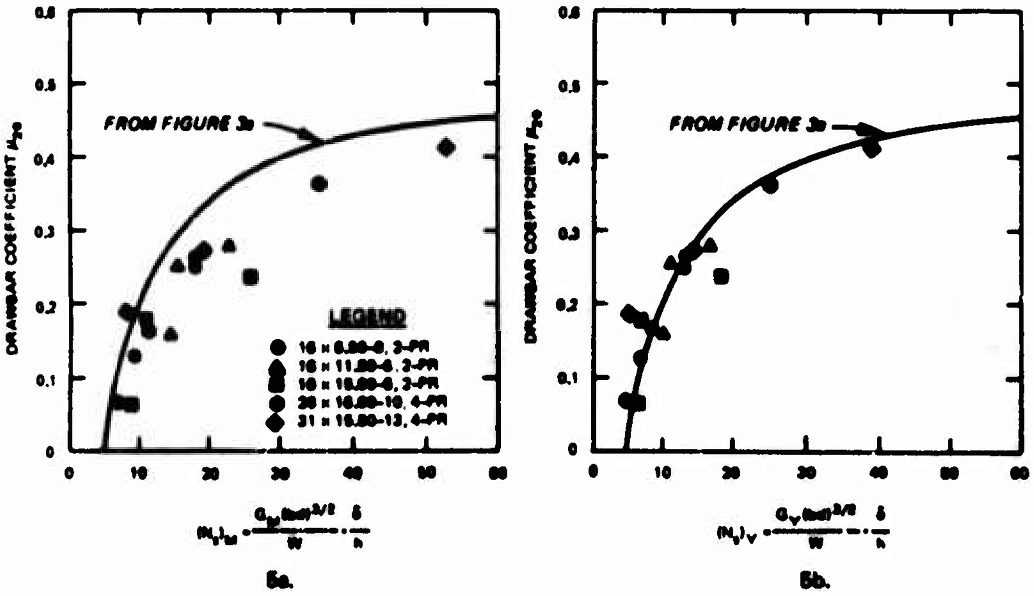

Figure 5. Effect of converting G_M to G_Y in the relation of μ_{20} to N_s for tires operating at 20 percent slip in mortar sand

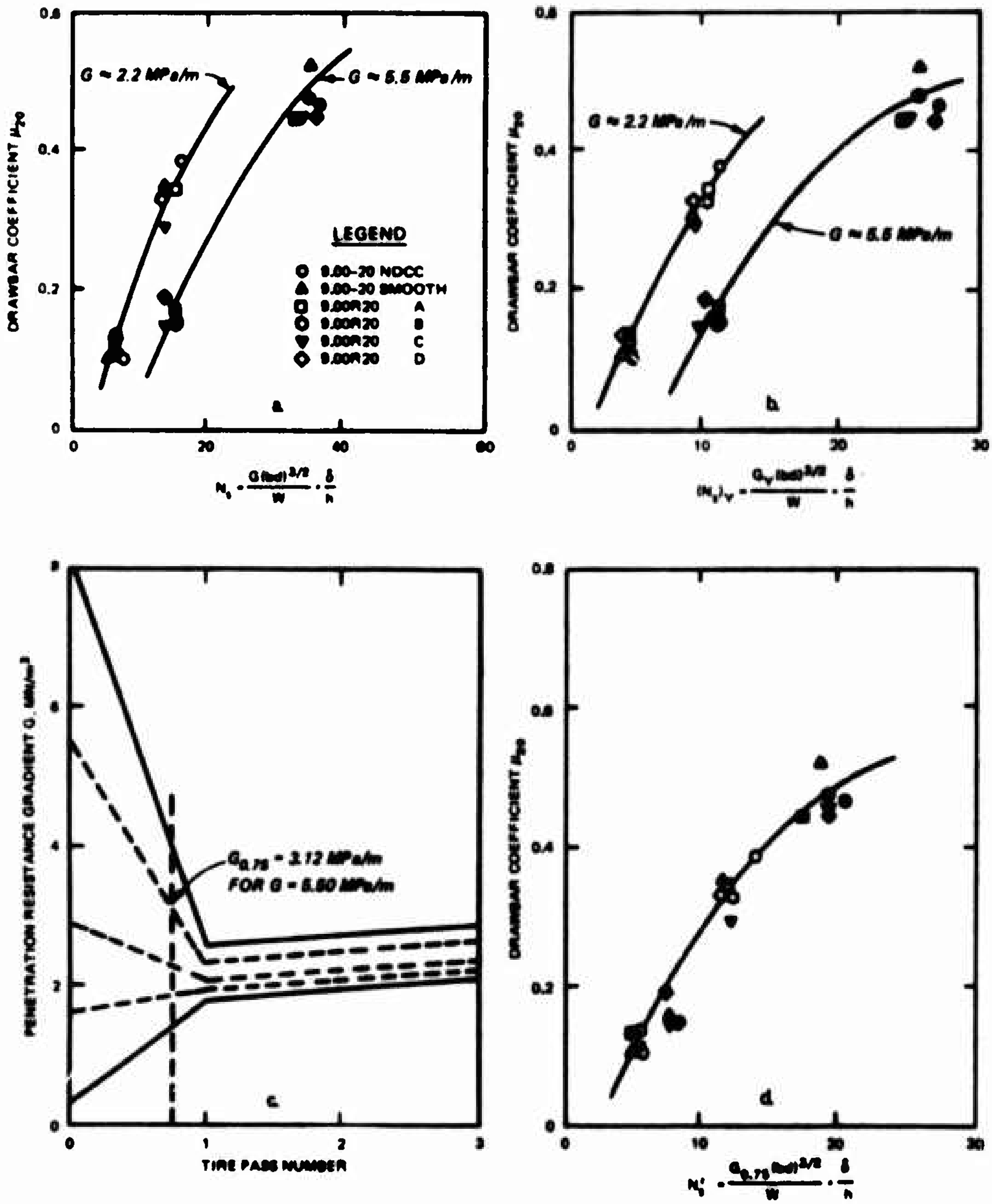

NOTE: OPEN SYMBOLS ARE FOR G=2.2MPa/m; CLOSED FOR G=5.5MPa/m

Figure 6. Relations of (a) μ_{20} to N_s, (b) μ_{20} to $(N_s)_y$, (c) G to tire pass number, and (d) μ_{20} to N'_s for tests of six 9.00x20 tires in mortar sand

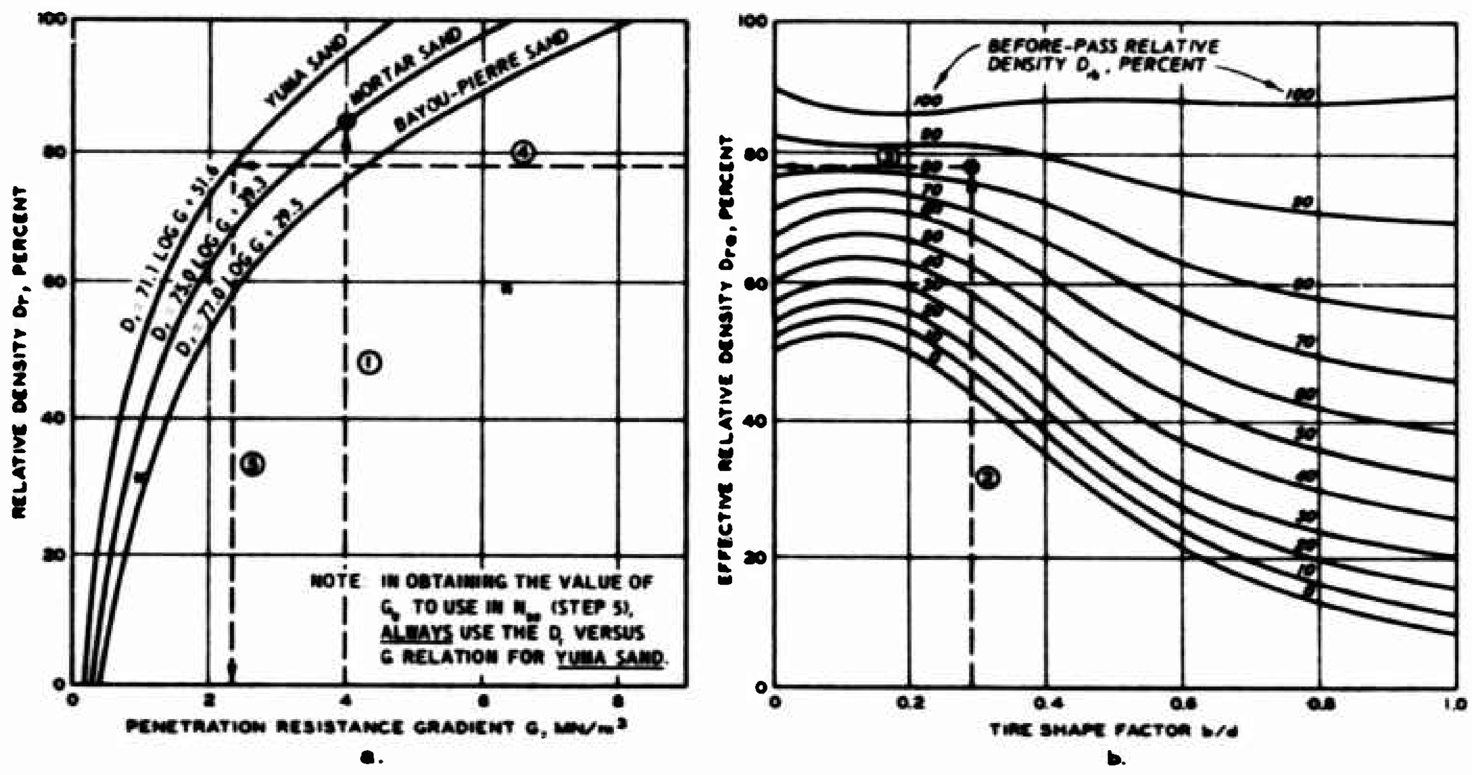

Figure 7. (a) Relations of D_r to G for three sands, and (b) from Reference 8, tentative relations among b/d, D_{rb}, and D_{re} for sands in general (subsequently replaced by relations developed herein)

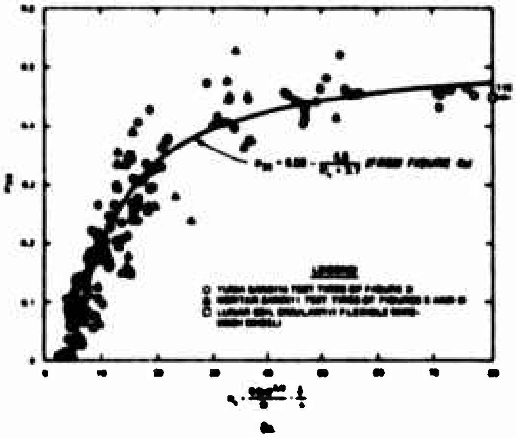

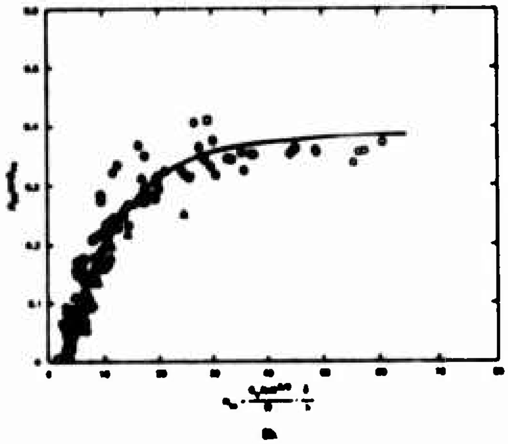

Figure 8. Relations of (a) μ_{20} to N_s and (b) μ_{20} tan ϕ_{70} to N_{se} for the three frictional test soils considered in Reference 8

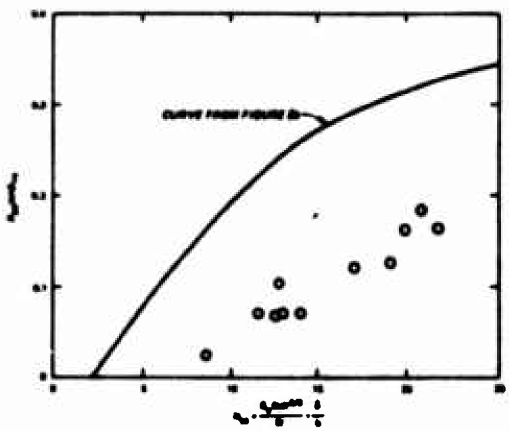

Figure 9. Relation of μ_{20} tan ϕ_{70} to N_{se} for 6.00-16, 2-PR tire tested in air-dry Cresswell sand (adapted from Reference 11)

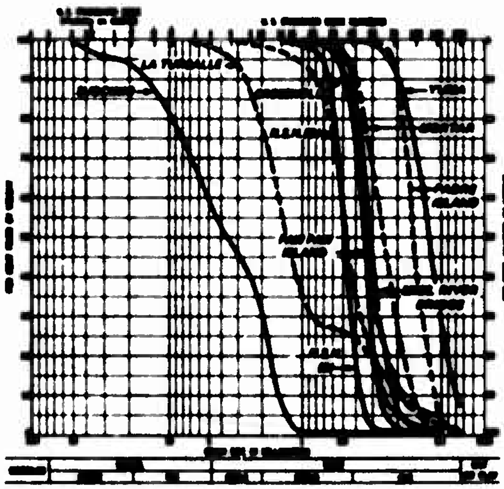

Figure 10. Grain size distributions of ten sand samples analyzed at WES in 1983

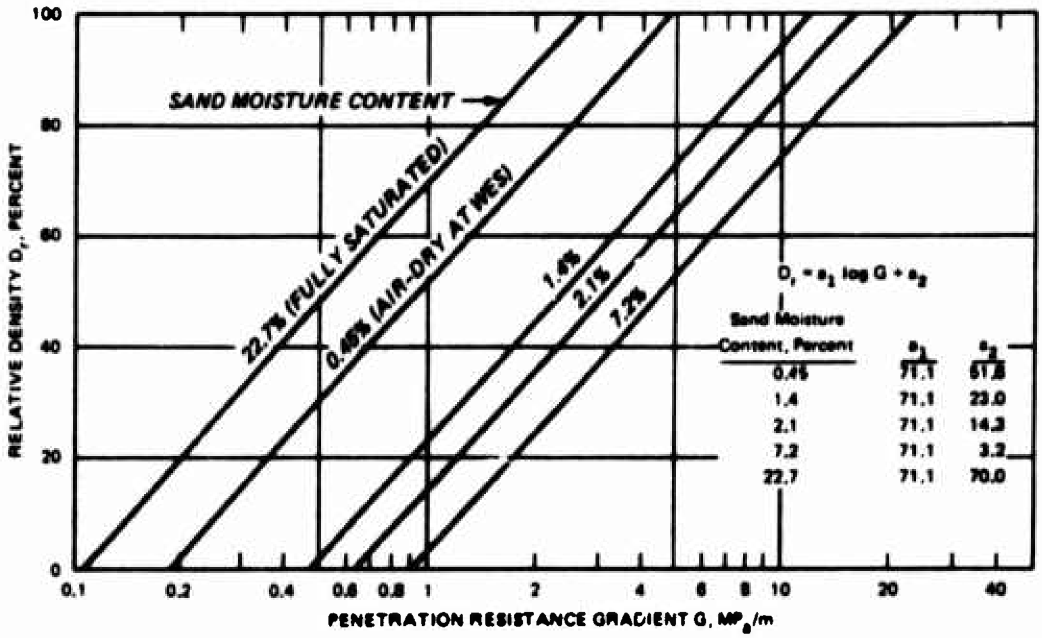

Figure 11. Relations among G, D_r, and sand moisture content for Yuma sand

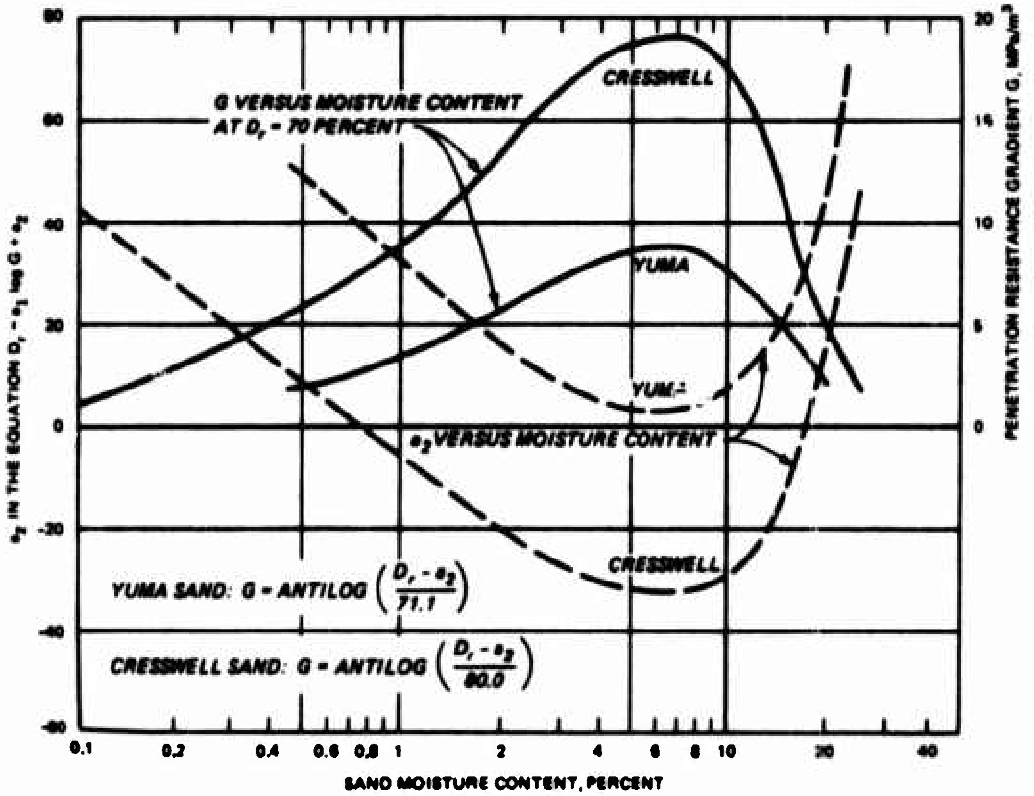

Figure 12. Relations of (a) a_2 to sand moisture content and (b) G at D_r = 70 percent to sand moisture content for Yuma and Cresswell sands

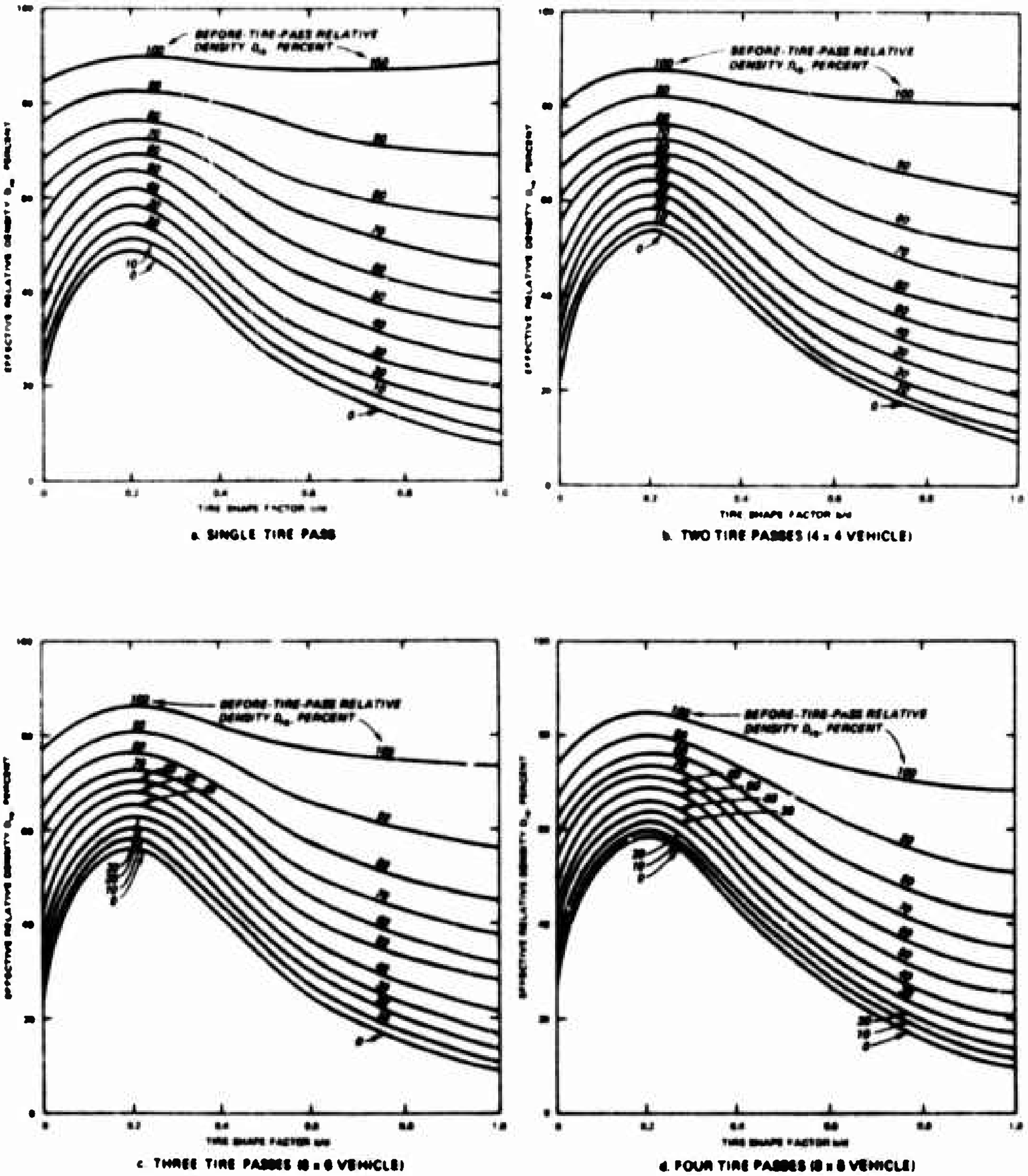

Figure 13. Relations among D_{rb} , b/d , and D_{re} for one, two, three, and four tire passes in sand (at 20 percent slip with tire deflection in the 15 to 35 percent range)

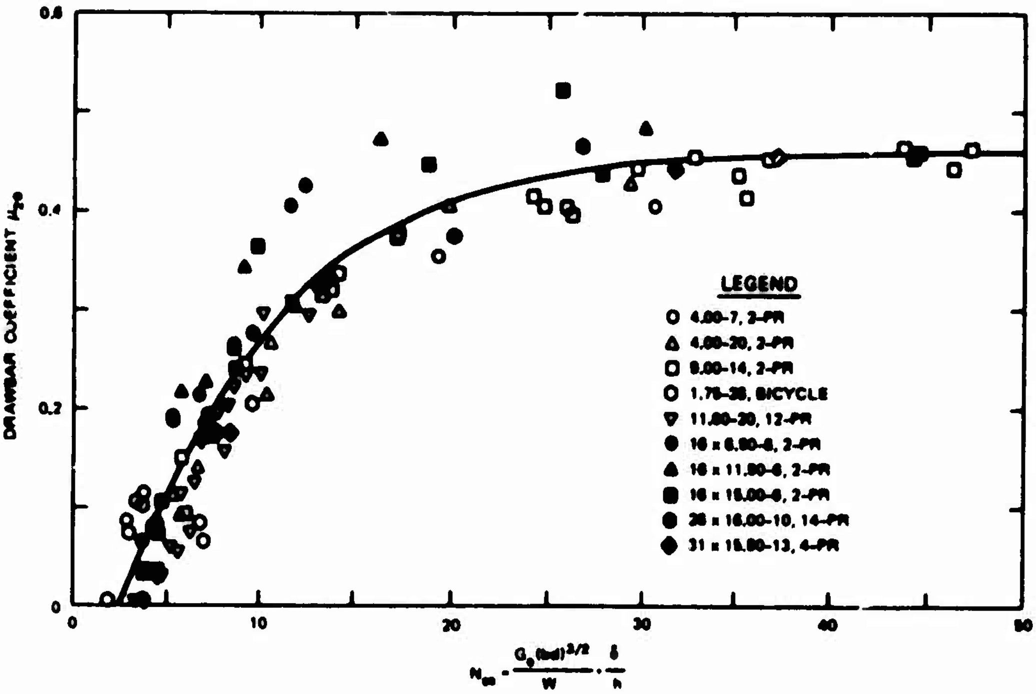

a.

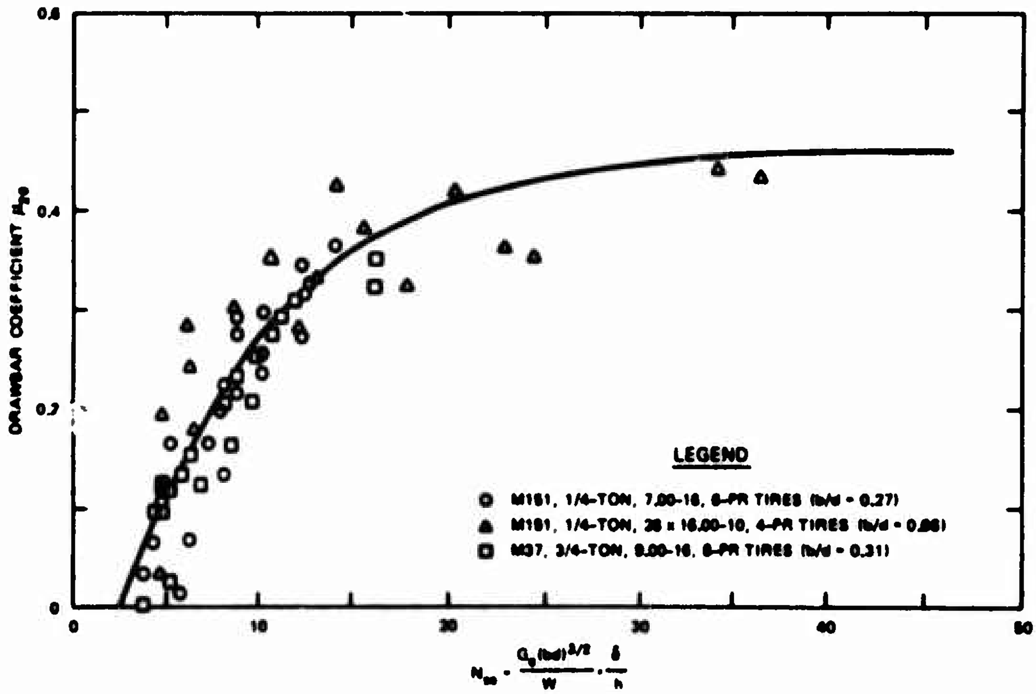

b.

Figure 14. Single relation of μ_{20} to N_{se} (a) for ten single tires and (b) for three 4x4 vehicles, each tested in air-dry Yuma sand

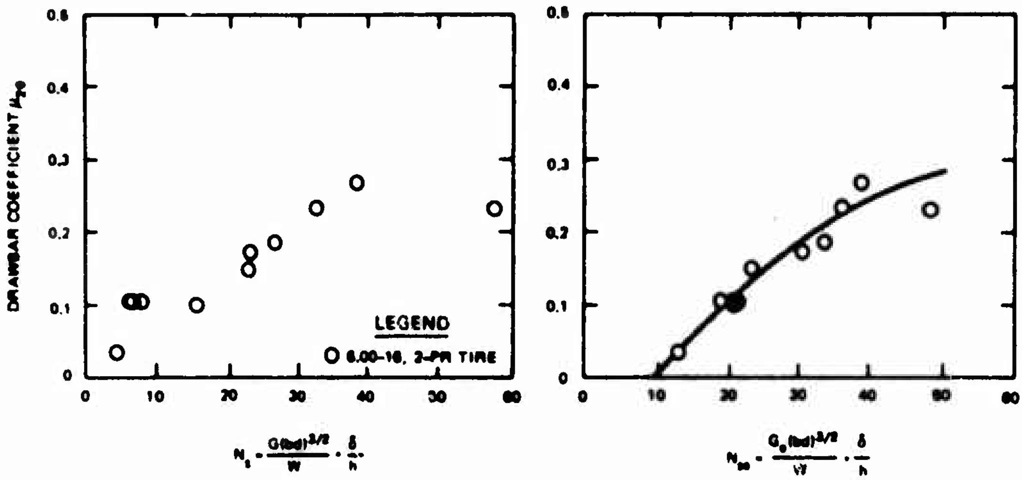

a. CRESSWELL SAND

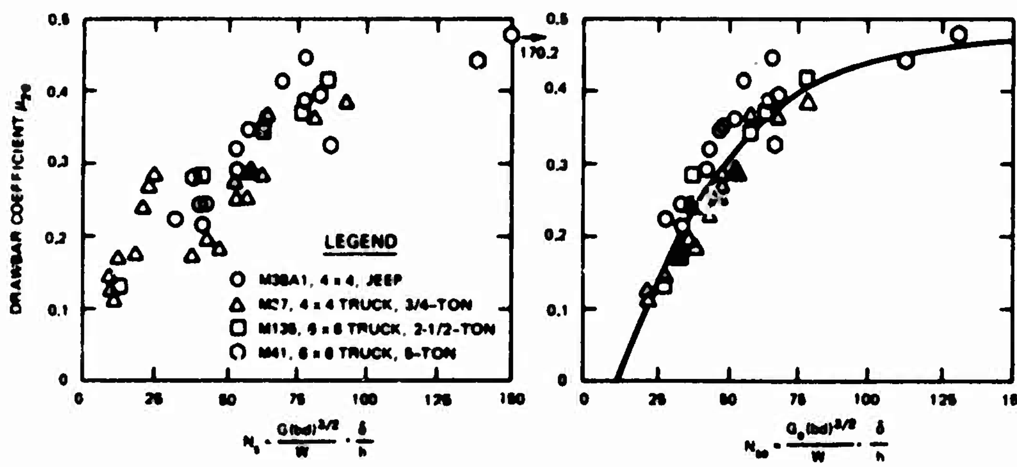

b. PADRE ISLAND SAND

Figure 15. Relations of μ_{20} to N_s and μ_{20} to N_{se} (a) for the 6.00-16, 2-PR tire in air-dry Cresswell sand, and (b) for four wheeled vehicles in moist Padre Island sand

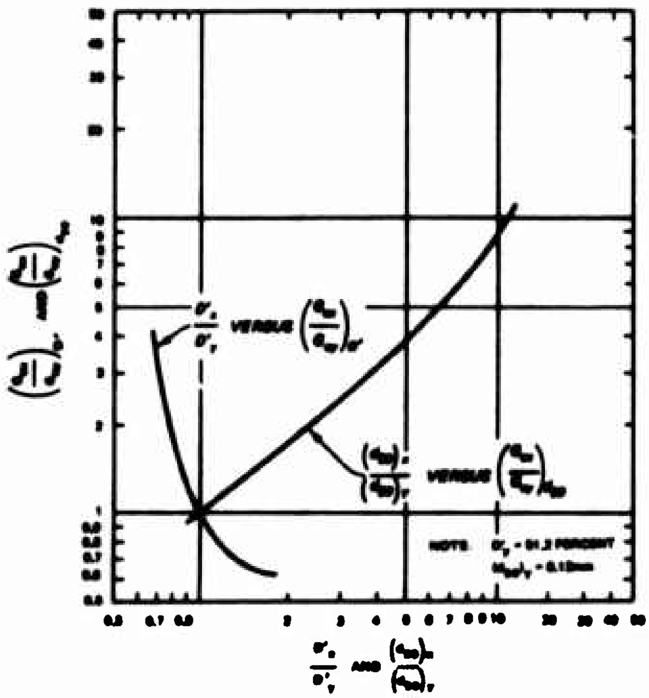

Figure 16. Relations of $\frac{D'_x}{D'_y}$ to $\left(\frac{G_{ex}}{G_{ey}}\right)_{D'}$ and

$$\frac{(d_{50})_x}{(d_{50})_y} \text{ to } \left(\frac{G_{ex}}{G_{ey}}\right)_{d_{50}}$$

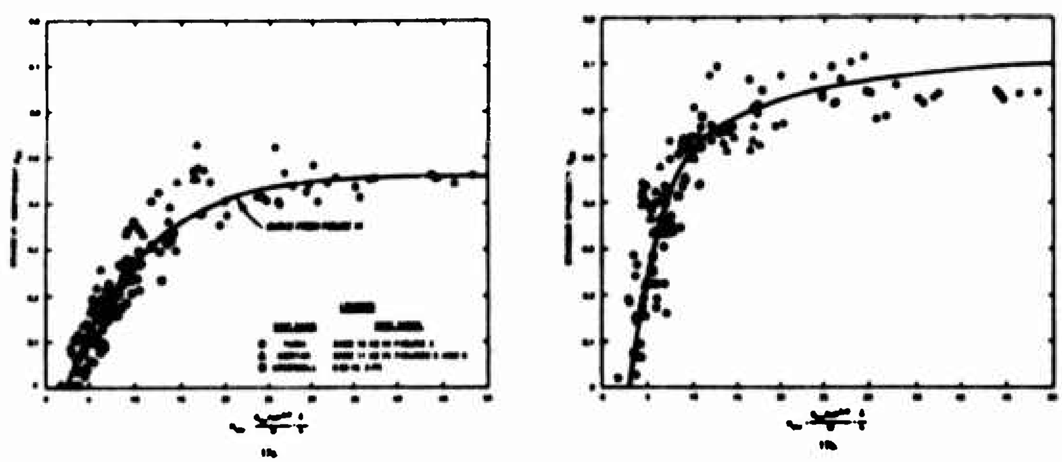

Figure 17. Relations of (a) μ_{20} to N_{sey} and (b) η_{20} to N_{sey} for single-tire tests in air-dry Yuma, mortar, and Cresswell sands

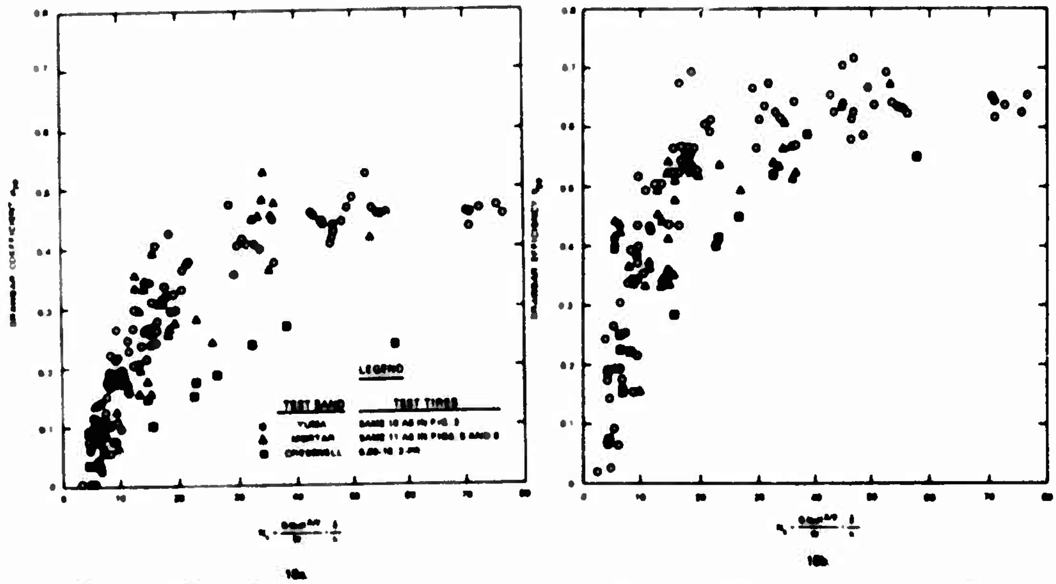

Figure 18. Relations of (a) μ_{20} to N_s and (b) η_{20} to N_s for single-tire tests in air-dry Yuma, mortar, and Cresswell sands

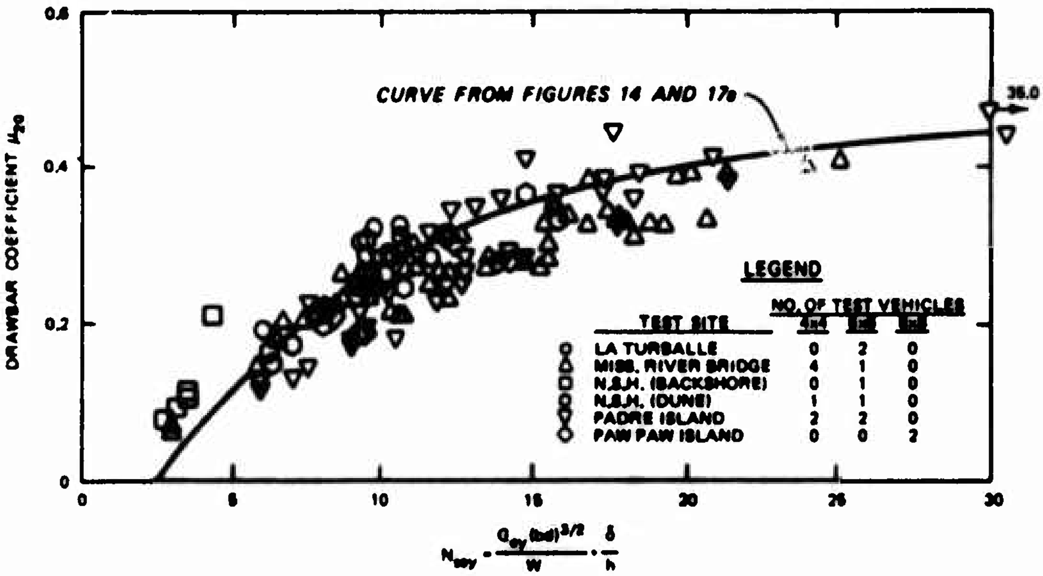

Figure 19. Relation of μ_{20} to N_{sey} for tests with a variety of wheeled vehicles at six sandy field sites

Table 1

Comparison of Grain Diameters of 10 Sands from Original Test Reports and from 1983 WES Laboratory Tests

Sand	$(d_{10})_{orig.} / (d_{10})_{1983}$ *	$(d_{30})_{orig.} / (d_{30})_{1983}$	$(d_{50})_{orig.} / (d_{50})_{1983}$	$(d_{70})_{orig.} / (d_{70})_{1983}$	$(d_{90})_{orig.} / (d_{90})_{1983}$	Reference No. of Original Test Report
Cresswell	0.32/0.26	0.40/0.31	0.45/0.34	0.59/0.39	0.90/0.50	11
La Turbalie**	0.48/0.24	0.97/0.86	1.45/1.30	1.75/1.80	2.80/2.70	12
Mississippi River Bridge	0.16/0.21	0.22/0.27	0.26/0.31	0.30/0.36	0.37/0.41	12
Mortar	0.17/0.17	0.22/0.20	0.25/0.25	0.30/0.30	0.35/0.39	4,6
N.S.H.† (backshore area)	0.39/0.36	0.50/0.42	0.57/0.49	0.65/0.54	0.81/0.64	12
N.S.H. (dune area)	0.17/0.20	0.31/0.37	0.56/0.47	0.96/0.56	4.00/0.79	12
Padre Island	0.11/0.11	0.15/0.14	0.16/0.15	0.18/0.18	0.21/0.20	12
Paw Paw Island	0.19/0.19	0.27/0.27	0.32/0.32	0.38/0.38	0.49/0.49	13
Suscinio**	0.56/1.50	1.45/2.00	2.45/3.50	4.40/7.00	9.60/16.00	12
Yuma	0.08/0.08	0.10/0.10	0.12/0.12	0.14/0.16	0.19/0.20	4,6

* All d values are in mm, and were obtained from plots such as those in Figure 10.

** For the La Turballe and the Suscinio test sites, each d value listed above from the original test report is the average of d values from similar grain-size distributions for two test areas at that site—a foreshore test area and a backshore test area.

† N.S.H. is National Seashore Headquarters, the agency in Massachusetts that presently occupies the test area occupied by Camp Wellfleet when the wheeled vehicle tests of Reference 12 were conducted.

Table 2

WES Measurements of Some Key Sand Parameters Related to In-Sand Drawbar Performance

(1)	(2)	(3)	(4)	(5)	(6)	(7)	(8)	(9)	(10)	(11)	(12)	(13)	(14)	(15)
		In $D_r = a_1 \log G + a_2$							Maximum Void Ratio	Minimum Void Ratio		Median Grain Diameter		
	At-WES Air-Dry Moisture	Constant	*a_2 at Moisture Content of								Compac-tibility			
Sand	Content, %	a_1	Air-Dry	0.5 %	1 %	2 %	3 %	7 %	e_{max}	e_{min}	D', %	d_{50}, mm	$\frac{D'_x}{D'_y}$	$\frac{(d_{50})_x}{(d_{50})_y}$
Cresswell	0.22	80.0	+26.0	+8.0	-6.0	-20.5	-27.0	-30.5	0.782	0.548	42.7	0.34	0.83	2.83
La Turballe	0.20	60.0	+35.5	+16.5	+2.7	-11.0	-15.5	-18.0	0.630	0.345	82.6	1.30	1.61	10.80
Mississippi River Bridge	0.20	115.8	+25.3	-12.7	-41.0	-69.0	-82.0	-90.0	0.732	0.532	37.6	0.31	0.73	2.58
Mortar	0.08	75.0	+39.3	+29.0	-1.0	-13.0	-19.5	-25.0	0.908	0.572	58.7	0.25	1.15	2.08
N.S.H. (backshore area)	0.16	134.5	+47.0	+6.0	-18.5	-43.3	-55.5	-67.5	0.778	0.557	39.7	0.49	0.78	4.08
N.S.H. (dune area)	0.12	116.7	+27.0	-12.5	-31.5	-50.5	-56.0	-58.5	0.685	0.466	47.0	0.47	0.92	3.92
Padre Island	0.13	132.6	+40.7	-24.5	-54.5	-84.0	-94.0	-103.0	0.813	0.596	36.4	0.15	0.71	1.25
Paw Paw Island	0.32	65.0	+39.0	+33.0	+26.5	+18.0	+14.5	+11.5	0.839	0.518	62.0	0.32	1.40	2.67
Suscinio	0.12	141.0	+27.0	-1.0	-14.5	-26.5	-30.0	-33.0	0.528	0.380	38.9	3.50	0.76	29.20
Yuma	0.45	71.1	+51.6	+49.5	+31.5	+15.2	+9.2	+3.5	0.919	0.608	51.2	0.12	1.00	1.00

* a_2 values for the air-dry moisture contents of column 2 were obtained in tests at the particular moisture content values indicated. a_2 values for moisture contents of 0.5, 1, 2, 3, and 7 percent were obtained from curves similar to those in Figure 12.

Table 3

Comparison of G_{ey} Values Obtained for Air-Dry Cresswell Sand from Two Sets of Input Values of a_1, a_2, D', and d_{50}

(1) Test No.	(2) μ_{20}	(3) η_{20}	(4) N_s	(5) G, MPa m	(6) D_{rb},* %	(7) D_{re} %	(8) G_{ex}, MPa m	(9) G_{ey}, MPa m	(10) N_{sey}	(11) D_{rb},** %	(12) D_{re}, %	(13) G_{ex}, MPa m	(14) G_{ey}, MPa m	(15) N_{sey}
1	0.035	0.074	4.7	0.78	39.4	61	2.06	0.60	3.6	17.4	53	2.18	0.58	3.5
2	0.102	0.250	6.4	0.65	35.3	60	1.97	0.57	5.6	11.0	52	2.11	0.56	5.5
3	0.102	0.225	6.7	0.78	39.4	61	2.06	0.60	5.2	17.4	53	2.18	0.58	5.0
4	0.102	0.220	8.1	0.82	40.5	62	2.15	0.62	6.1	19.1	54	2.24	0.59	5.8
5	0.100	0.282	15.6	2.58	66.0	71	3.23	0.94	5.7	48.9	69	3.45	0.91	5.5
6	0.150	0.400	22.7	3.76	74.4	74	3.69	1.07	6.5	72.0	74	3.98	1.05	6.3
7	0.174	0.413	23.0	2.59	66.1	71	3.23	0.94	8.3	59.1	69	3.45	0.91	8.1
8	0.185	0.450	26.5	2.68	66.9	71	3.23	0.94	9.3	60.3	69	3.45	0.91	9.0
9	0.236	0.520	32.5	3.29	71.4	74	2.53	1.02	10.1	67.4	71	3.65	0.97	9.6
10	0.268	0.588	38.4	3.89	75.2	75	3.86	1.12	11.1	73.2	74	3.98	1.05	10.4
11	0.234	0.550	57.9	6.53	86.7	80	4.83	1.40	12.4	91.2	85	5.46	1.44	12.8

* Note that $D_{rb} = a_1 \log G + a_2$; D_{re} is obtained from Figure 13; $G_{ex} = \text{antilog} \dfrac{D_{re} - a_2}{a_1}$; and $G_{ey} = G_{ex} \div \dfrac{G_{ex}}{G_{ey}}$. For columns 6-10, the following input data values were used: $a_1 = 51.3$, $a_2 = 44.9$, $d_{50} = 0.45$ mm (from References 10 and 11), and $D' = 47.6$ percent (from Reference 14). (These D' and d_{50} values produced a $\dfrac{G_{ex}}{G_{ey}}$ value from Figure 16 of 3.45.)

** For columns 11-15, the following input data values were used from 1983 WES soils laboratory testing: $a_1 = 80.0$, $a_2 = 26.0$, $D' = 42.7$ percent, and $d_{50} = 0.34$ mm. (These D' and d_{50} values produced a $\dfrac{G_{ex}}{G_{ey}}$ value of [illegible].)